Xianxian Yu
Key Laboratory for Mechanics in Fluid Solid Coupling Systems,
Institute of Mechanics,
Chinese Academy of Sciences,
No. 15 of Beisihuanxi Road,
Beijing 100190, China

Chenguang Huang
Key Laboratory for Mechanics in Fluid Solid Coupling Systems,
Institute of Mechanics,
Chinese Academy of Sciences,
No. 15 of Beisihuanxi Road,
Beijing 100190, China

Tezhuan Du
Key Laboratory for Mechanics in Fluid Solid Coupling Systems,
Institute of Mechanics,
Chinese Academy of Sciences,
No. 15 of Beisihuanxi Road,
Beijing 100190, China

Lijuan Liao
Key Laboratory for Mechanics in Fluid Solid Coupling Systems,
Institute of Mechanics,
Chinese Academy of Sciences,
No. 15 of Beisihuanxi Road,
Beijing 100190, China

Xiaocui Wu
Key Laboratory for Mechanics in Fluid Solid Coupling Systems,
Institute of Mechanics,
Chinese Academy of Sciences,
No. 15 of Beisihuanxi Road,
Beijing 100190, China

Zhi Zheng
School of Energy and Power Engineering,
Lanzhou University of Technology,
Lanzhou, Gansu 730050, China

Yiwei Wang[1]
Key Laboratory for Mechanics in Fluid Solid Coupling Systems,
Institute of Mechanics,
Chinese Academy of Sciences,
No. 15 of Beisihuanxi Road,
Beijing 100190, China
e-mail: wangyw@imech.ac.cn

Study of Characteristics of Cloud Cavity Around Axisymmetric Projectile by Large Eddy Simulation

Cavitation generally occurs where the pressure is lower than the saturated vapor pressure. Based on large eddy simulation (LES) methodology, an approach is developed to simulate dynamic behaviors of cavitation, using $k-\mu$ transport equation for subgrid terms combined with volume of fluid (VOF) description of cavitation and the Kunz model for mass transfer. The computation model is applied in a 3D field with an axisymmetric projectile at cavitation number $\sigma = 0.58$. Evolution of cavitation in simulation is consistent with the experiment. Clear understanding about cavitation can be obtained from the simulation in which many details and mechanisms are present. The phenomenon of boundary separation and re-entry jet are observed. Re-entry jet plays an important role in the bubble shedding. [DOI: 10.1115/1.4026583]

Keywords: cloud cavity, large eddy simulation, re-entrant jet, shedding bubble

1 Introduction

Cavitation can be defined as the breakdown of a liquid medium under very low pressure [1]. Most vehicles handling liquids are exposed to cavity, such as high-speed torpedoes, hydrofoils, propellers, etc. Under certain conditions, cavity exhibits unsteady dynamic behavior, such as the periodic shedding of vapor cloud. The relative collapse of the vapor cloud, especially in the cloud cavitation, is often responsible for the generation of loud noise and erosion damage [2].

Cavitation, as a critical phenomenon, has been attractive in the past decades. In earlier times, most computational study on cavitation was based on Reynolds-averaged Navier–Stokes (RANS) equations. Based on the motion model of bubbles put forward by Rayleigh et al., Plesset and Prosperetti [3] established the Rayleigh–Plesset model, which analyzed the dynamic behavior of bubble in cavitation effectively. Singhal et al. [4] set up the

[1]Corresponding author.

Contributed by the Fluids Engineering Division of ASME for publication in the Journal of Fluids Engineering. Manuscript received April 3, 2013; final manuscript received January 14, 2014; published online March 17, 2014. Assoc. Editor: Olivier Coutier-Delgosha.

full-cavitation model, which accounts for the formation and transport of vapor bubbles, the turbulence of fluctuations of pressure and velocity, and the magnitude of noncondensable gases. The phase-change rate expressions are derived from a reduced form of Rayleigh–Plesset equation. Having adopted in commercial software FLUENT, this model is widely used today. Dular et al. [5] performed an experimental and numerical study of developed cavitating flow around hydrofoil, using particle image velocimetry-laser induced fluorescence (PIV-LIF) technology and the software FLUENT. Comparison made between numerical and experimental results showed good correlation in velocity fields, pressure coefficient, cavity length, shedding frequencies, etc. Both in simulation and experiment, significant backflow is predicted. However, it revealed little mechanism in cavitation. Huang et al. [6] made evaluation of Kubota, Singhal, Merkle, and Kunz cavitation models through calculation of cloud cavitation. The four models, which have difference in the cavity's length, velocity field, drag, etc., all can capture the form and shedding of cavity well. Ji et al. [7] simulated the unsteady cavitating flow around a twisted hydrofoil by adopting a specialized filter-based turbulence model and homogenous cavitation model. Two kinds of cavities shedding, i.e., primary shedding and secondary shedding, were noted, which resulted from the re-entrant jet and the side entrant jet, respectively, under certain conditions.

Recently, there are many cavitating researches adopting large eddy simulation (LES) model. In LES, the large, energy-containing structures are resolved on the computational grid, whereas the smaller, more isotropic, subgrid structures are modeled; this separation of scales within the flow is accomplished by a low-pass filtering of the Navier–Stokes equations [8].Compared with RANS approach, which is based on average flow description with the possibility of missing some details of flow field, LES consistently allows for medium-scale to small-scale transient flow structures and could capture certain mechanisms in the development of cavitation. Bensow and Bark [8,9] adopted an implicit LES method to describe dynamic cavitation behavior around the NACA0015 foil, Delft Twist11 foil, and the INSEANE779A propeller in a wake flow. They believed that LES would become a useful and reliable tool to study the details of cavitation flow field, but LES also needs further development. Wang and Ostoja-Starzewski [10] employed LES scheme combined with a fifth-order polynomial curve, which described the relationship between density coefficient ratio and pressure coefficient, to simulate the sheet/cloud cavitation around NACA0015 hydrofoil. In their study, time-dependent sheet/cloud cavitation structures under different attack angles and cavitation number were researched.

In this paper, the evolution of cloud cavitation around an axisymmetric vehicle is studied, using LES method together with transport equation for local volume fraction of vapor and the Kunz model for mass transport. Contrasted with experimental results, many details and mechanisms of the flow field are captured during evolution of cloud cavitation, e.g., re-entrant flow, separation of boundary, and movement of shedding bubbles.

2 Numerical Simulation

2.1 LES Method. In turbulent flow, large-scale eddy structures are anisotropic, while smaller ones are more isotropic. The essential issue of LES is that the large- and small-scale eddies are solved from the instantaneous Navier–Stokes equations and the subgrid stress (SGS) model, respectively.

The Navier–Stokes equations of incompressible flow are as follows:

$$\nabla \cdot (\rho \mathbf{v}) = 0 \tag{1}$$

$$\frac{\partial}{\partial t}(\rho \mathbf{v}) + \nabla \cdot (\rho \mathbf{v}\mathbf{v}) = -\nabla p + \nabla \cdot \mathbf{S} \tag{2}$$

where ρ, $\mathbf{v}$, and p are density of the mixture, velocity, and pressure, respectively, and $\mathbf{S} = 2\mu\mathbf{D}$ means the viscous stress tensor.

In LES, ψ is decomposed into large-scale quantity $\bar{\psi}$ and small-scale quantity ψ'. $\bar{\psi}$ can be expressed as follows:

$$\bar{\psi} = \int_{-\infty}^{+\infty} \psi G(x, x')dx' \tag{3}$$

where $\mathbf{G} = \mathbf{G}(x, x')$ is the filter function. In this paper, the widely used top-hat filter function is adopted,

$$G(x, x') = \begin{cases} 1/\bar{\Delta} & |x - x'| \le \bar{\Delta}/2 \\ 0 & |x - x'| \le \bar{\Delta}/2 \end{cases} \tag{4}$$

where $\bar{\Delta} = \sqrt[3]{\Delta_x \Delta_y \Delta_z}$ is spatial filter size. Δ_x, Δ_y, and Δ_z are the size of the grid in three directions.

By applying the above filter function to Navier–Stokes equations, the LES equations are derived as

$$\nabla \cdot (\rho \bar{\mathbf{v}}) = 0 \tag{5}$$

$$\frac{\partial}{\partial t}(\rho \bar{\mathbf{v}}) + \nabla \cdot (\rho \bar{\mathbf{v}}\bar{\mathbf{v}}) = -\nabla \bar{p} + \nabla \cdot (\bar{\mathbf{S}} - \mathbf{B}) \tag{6}$$

where the overbar denotes the low-pass–filtered dependent variables. $\bar{\mathbf{S}} = 2\mu\bar{\mathbf{D}}$ is the filtered viscous stress tensor, $\bar{\mathbf{D}} = 1/2\left(\nabla\bar{\mathbf{v}} + \nabla\bar{\mathbf{v}}^T\right)$ stands for the filtered rate of stress tensor, and μ is the dynamic viscosity. $\mathbf{B} = (\overline{\mathbf{v}\mathbf{v}} - \bar{\mathbf{v}}\bar{\mathbf{v}})$ means the subgrid stress tensor, representing the influence of the small, unresolved eddies on the larger, resolved ones. The commutation error terms expected to be significantly smaller than the subgrid terms are neglected.

Based on Boussinesq hypothesis, a subgrid viscosity μ_{SGS} is considered. The resulting term in the LES equations becomes $\mathbf{B} = -2\mu_{SGS}\bar{\mathbf{D}}$ so that the whole viscous term can be described as a function of the effective viscosity μ_{eff} (summation of the molecular viscosity μ and subgrid viscocity μ_{SGS}) and rate-of-strain tensor $\bar{\mathbf{D}}$, i.e., $\left(\bar{\mathbf{S}} - \mathbf{B}\right) = 2\mu_{eff}\bar{\mathbf{D}} = 2(\mu + \mu_{SGS})\bar{\mathbf{D}}$, where μ_{SGS} needs to be solved.

In the present paper, $k - \mu$ SGS model is applied to deal with the subgrid stress,

$$\frac{\partial k_{SGS}}{\partial t} + \nabla \cdot (k_{SGS}\bar{\mathbf{v}}) = \nabla \cdot \left[\frac{\mu + \mu_{SGS}}{\rho}\nabla k_{SGS}\right] + 2\frac{\mu_{SGS}}{\rho}\bar{\mathbf{D}}\,\bar{\mathbf{D}} - C_e\frac{k_{SGS}^{\frac{3}{2}}}{\bar{\Delta}} \tag{7}$$

$$\mu_{SGS} = C_k \rho \bar{\Delta}\sqrt{k_{SGS}} \tag{8}$$

where $C_\varepsilon = 1.048$ and $C_k = 0.094$.

2.2 Multiphase Modeling. Two phases, liquid and vapor, both exist in natural cavitating flows. To simulate cavitation, the two phases need to be described as well as the phase transition mechanism between them. In the paper, the VOF approach is considered, introducing the liquid volume fraction α. So the density and viscosity of fluid can be expressed by α [11],

$$\rho = \alpha\rho_l + (1 - \alpha)\rho_v \tag{9}$$

$$\mu = \alpha\mu_l + (1 - \alpha)\mu_v \tag{10}$$

where the subscripts l and v represent the water and vapor, respectively. Equation (10) describes the viscosity of the mixture, which is always simplified as the arithmetic mean of all the phases' dynamic viscosities in LES, such as in Refs. [8], [9], and [11] and the software FLUENT.

A transport equation for the volume fraction needs to be incorporated into the filtered equations of continuity and momentum, Eqs. (5) and (6).

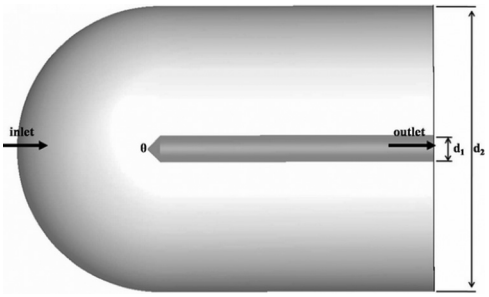

Fig. 1 Computational model and domain

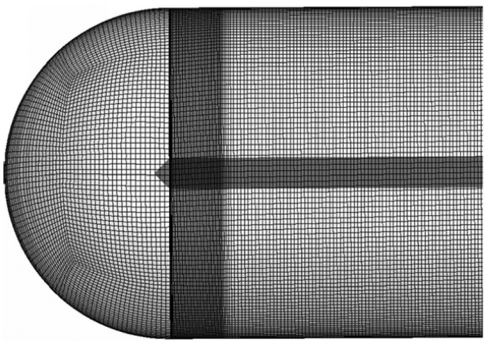

Fig. 2 Computational mesh

Table 1 Cavity form at different mesh number

Mesh number	5.4 ms	8.0 ms
2×10^6		
38×10^6	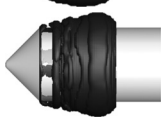	

$$\frac{\partial \alpha}{\partial t} + \nabla \cdot (\bar{\mathbf{v}}\alpha) = \frac{\dot{m}}{\rho_l} \tag{11}$$

$$\nabla \cdot (\rho \bar{\mathbf{v}}) = 0 \tag{12}$$

$$\frac{\partial}{\partial t}(\rho \bar{\mathbf{v}}) + \nabla \cdot (\rho \bar{\mathbf{v}}\bar{\mathbf{v}}) = -\nabla \bar{p} + \nabla \cdot (\bar{\mathbf{S}} - \mathbf{B}) \tag{13}$$

where $\dot{m}$, the mass transfer rate, is modeled by mass transfer model. Density of mixture ρ, which is not filtered here, is decided by vapor volume fraction α in VOF model. In cavitation, α is a macroscale quantity that requires a less-sophisticated model than others [12]. In transport equation of α, only the convection term contains obvious effect of velocity fluctuation. So in this equation, the filtered velocity is adopted directly. This approximate approach has been widely used, such as in Refs. [8] and [9].

2.3 Cavitation Modeling. Kunz model [13] is employed to model the mass transfer rate

$$\dot{m}^+ = \frac{C_v \rho_v \alpha \min[0, \bar{p} - p_v]}{(1/2\rho_l U_\infty^2) t_\infty} \tag{14}$$

$$\dot{m}^- = \frac{C_c \rho_v \alpha^2 (1 - \alpha)}{t_\infty} \tag{15}$$

The creation rate of vapor $\dot{m}^+$ is modeled to be proportional to the volume of liquid and the amount by which the pressure is below the vapor pressure. The destruction rate of vapor $\dot{m}^-$ is modeled as a third-order polynomial function of the liquid volume fraction when the pressure is above the vapor pressure.

2.4 Computational Model. Focused on the characteristics of cloud cavitation, a cylinder with cone angle $\theta = 90$ deg and diameter $d_1 = 37$ mm is adopted as the object to study, as shown in Fig. 1. The structured meshed computation domain, including this object, is prepared, as shown in Fig. 2. Diameter of the outside field is $d_2 = 400$ mm. Mesh independence should be examined to guarantee calculation accuracy. In Table 1, the cavity form and evolution progress are similar when the mesh number are 2×10^6 and 38×10^6. To take account of computational speed and accuracy together, the 2×10^6 case is chosen in the present paper [14].

The computational model described above has been realized through the open source code OPENFOAM. The undisturbed uniform velocity 18.5 m/s is given at the domain inlet, and the pressure is set as 1 atm at the domain outlet. The cavitation number $\sigma = 0.58$. For simulation presented in this paper, the first-order implicit

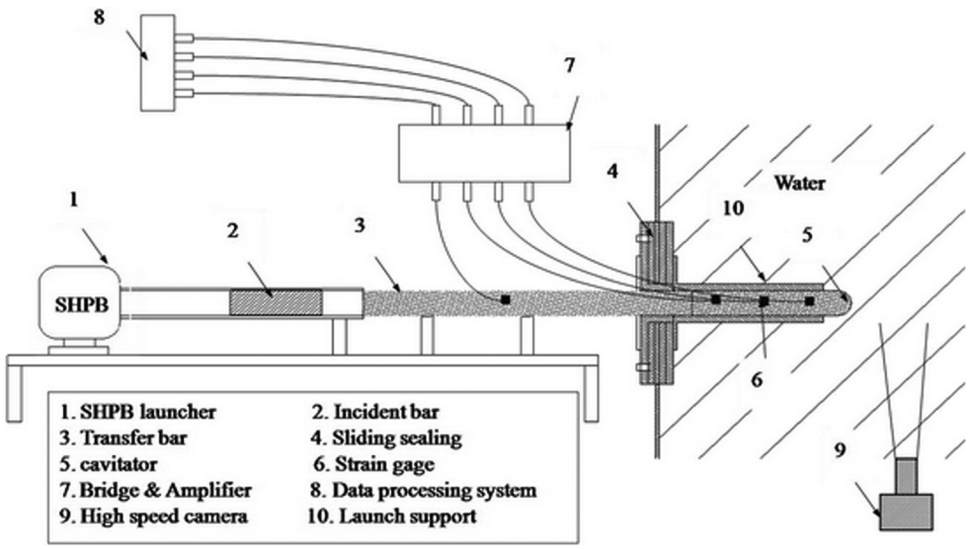

Fig. 3 Underwater launch system

Fig. 4 Projectile model in water tank

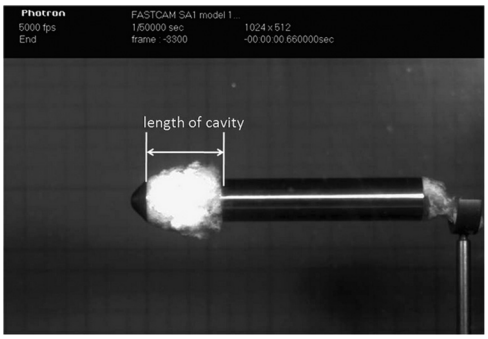

Fig. 5 Length of cavity in experimental picture at $t = 11.0$ ms

scheme is employed for time discretization and Gauss linear interpolation for spatial discretization. The time step is set as 0.1 μs with the maximum Courant number $C_o = 0.5$.

3 Experimental Device and Model

In order to verify the computational results, the experiment is carried out [15]. Split-Hopkinson pressure bar (SHPB) launching system is adopted in this paper. As shown in Fig. 3, the scaled underwater launch system mainly consists of four parts: the launching system (1, 2, 3, and 5), the water tank (4 and 10), the stain-sampling system (6, 7, and 8), and the high-speed camera (9). The launching system converted from SHPB is used to

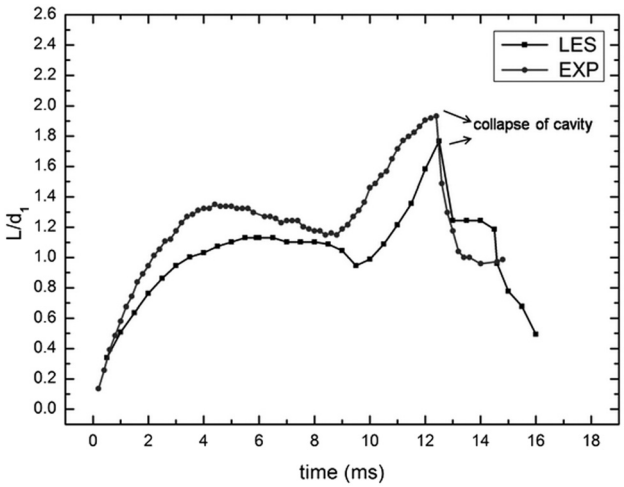

Fig. 7 Numerical and experimental results of cavity length

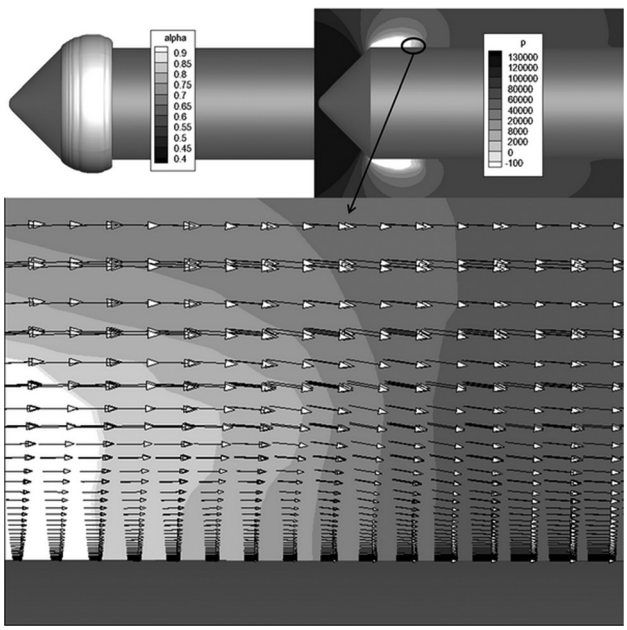

Fig. 8 Flow field of cavity closure at $t = 1.0$ ms

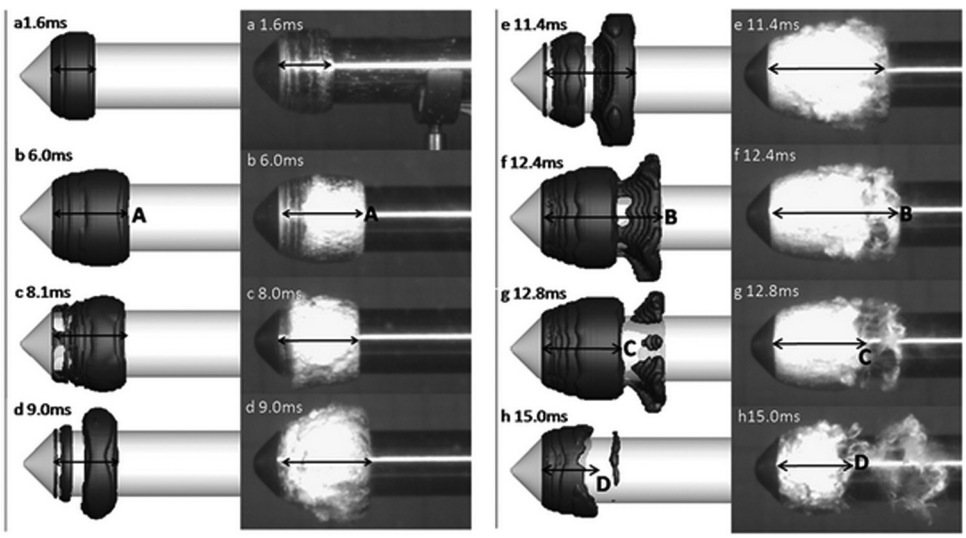

Fig. 6 Evolution of cloud cavitation

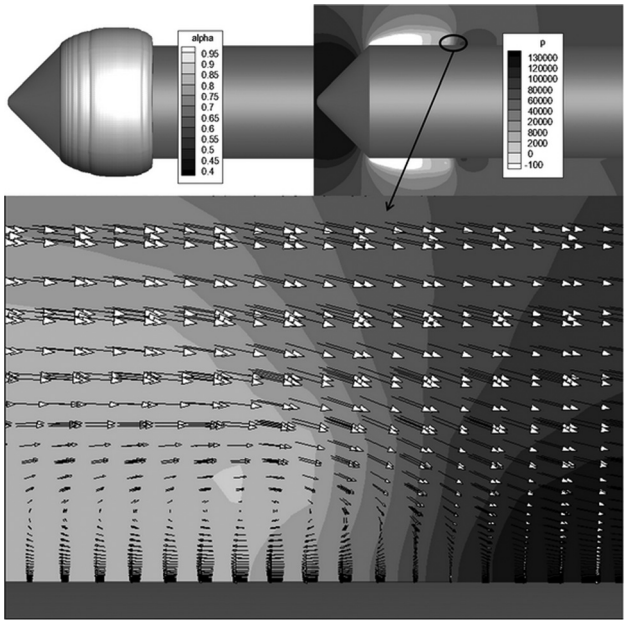

Fig. 9 Re-entry jet at the cavity closure at $t = 2.0$ ms

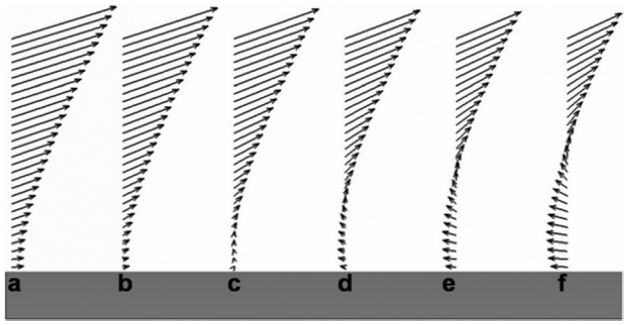

Fig. 10 Separation of boundary layer at $t = 2.0$ ms

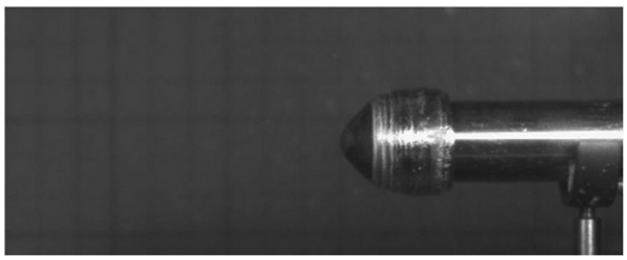

Fig. 11 The transparent cavity before re-entrant jet formed at $t = 2.2$ ms

accelerate the incident bar. The stress-wave signal traveling in the transmission bar and projectile can be obtained from the strain-sampling system. The high-speed camera is used to capture the trajectory and cavitations' features.

One-dimensional stress-wave theory is employed here to analyze the process of the energy transmission in the system. Details can be obtained in Ref. [15]. By the stress wave generated from SHPB, the experimental system can accelerate the body transiently to 30 m/s in less than 200 μs with slight disturbance during the whole process. Corresponding to the simulation model, the polished stainless steel projectile model is a 246 mm slender cylinder with 37 mm diameter and 90 deg conical angle, as shown in Fig. 4.

From pictures, we can get some information about the process. For example, a projectile in which the length is 246 mm is about

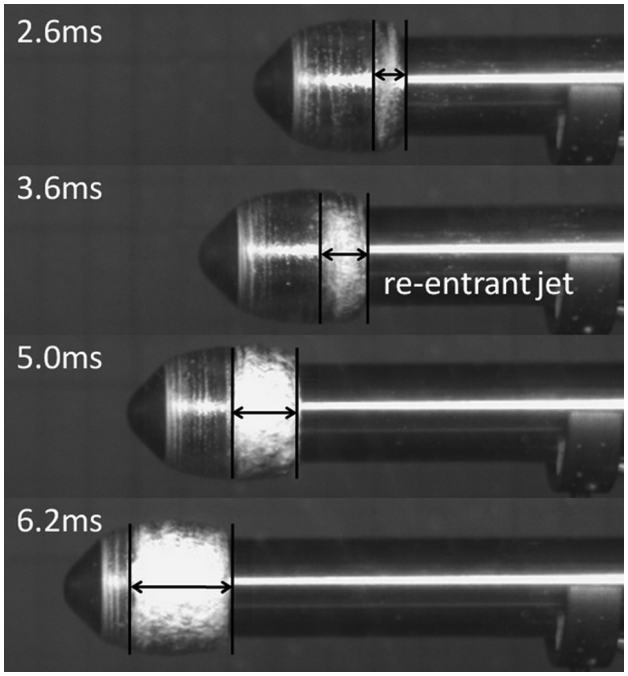

Fig. 12 Re-entrant jet in experiment

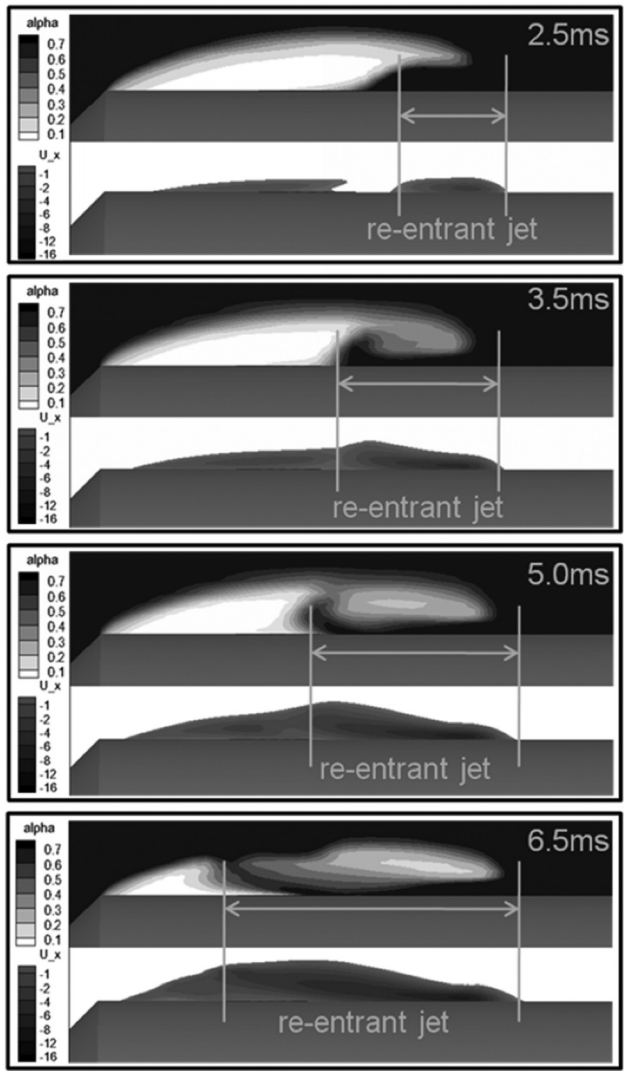

Fig. 13 Re-entrant jet in simulation

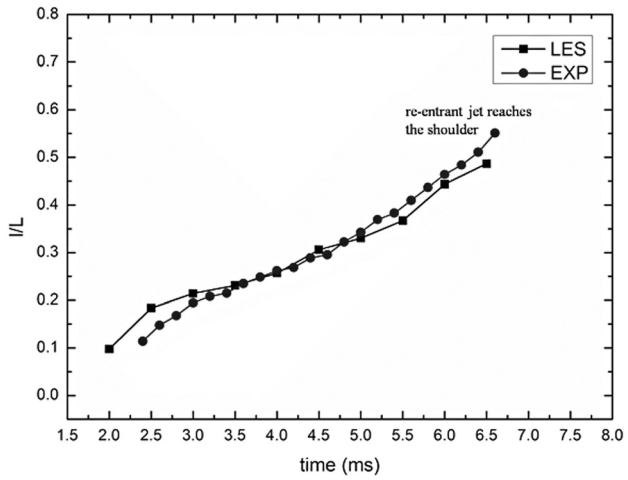

Fig. 14 Numerical and experimental *l/L*

490 pixels in axial direction in pictures. Then, 1 pixel stands for 0.50 mm, and the deviation is 0.50 mm too. As shown in Fig. 5, we can get the lengths of the cavity through measuring the pixels in pictures.

4 Results and Discussion

4.1 Evolution of Natural Cavitation. The numerical and experimental evolutions of natural cavitation are shown in Fig. 6. The evolution can be described as follows.

After the projectile is launched, the flow speed is relatively high at the shoulder where pressure decreases rapidly. When the pressure is lower than the saturation vapor pressure, water begins to vaporize. Then, the cavity forms and grows gradually, as shown in Fig. 6(*a*). At the same time, under adverse pressure gradient near the closure of the cavity, re-entry jet appears and flows back to the forepart of the projectile, as shown in Fig. 6(*b*). When the re-entry jet arrives at the shoulder of the projectile, the primary cavity separates from the body as a whole, as shown in Figs. 6(*c*) and 6(*d*). Then, the shedding bubble moves to the tail of the projectile with the main flow, becomes smaller, and collapses at last. Meanwhile, new cavity appears at the shoulder again and repeats the evolution described above. That is the periodic characteristic of natural cavitation evolution.

The length of cavity is *L*. Cavity is thought to start from the shoulder of the projectile in the present paper. It is easy to decide where the cavity closes when the cavity is a whole. For example, in Fig. 6(*b*), the cavity closes at A. When the cavity separates totally and the shedding part becomes smaller and smaller, the cavity is thought to close at the tail of the forepart. For example,

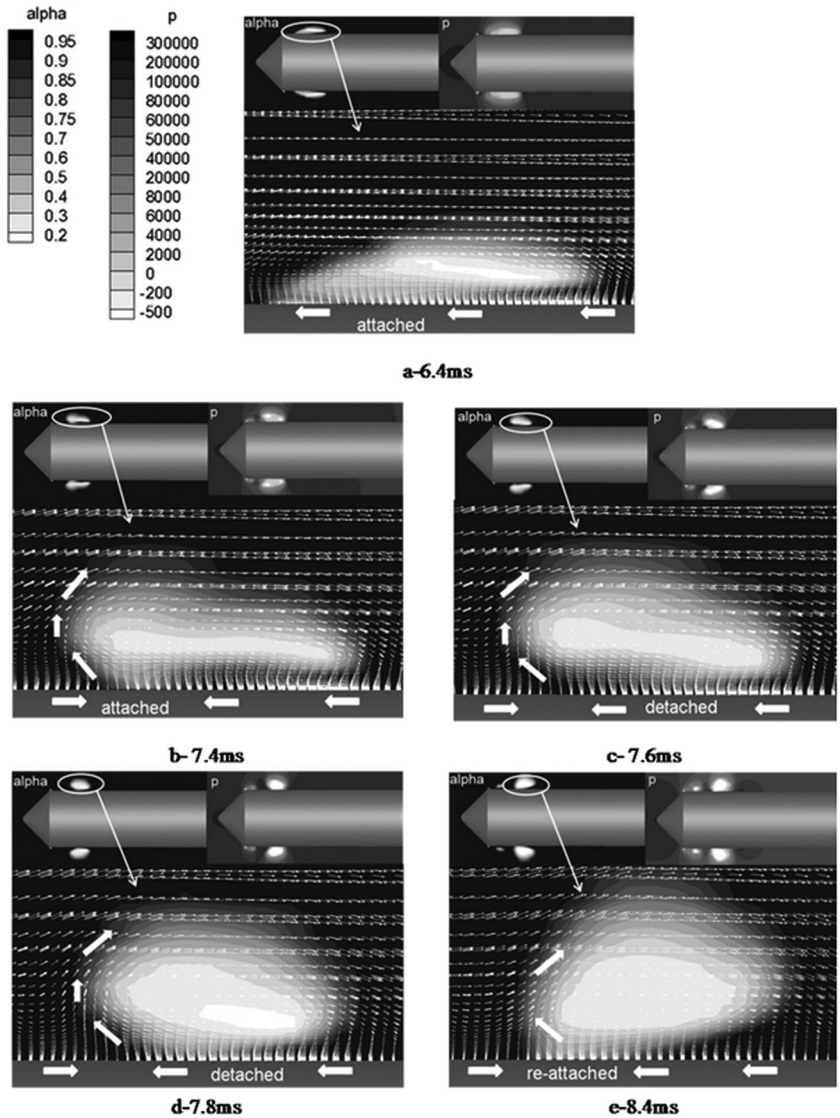

Fig. 15 Evolution of shedding bubble

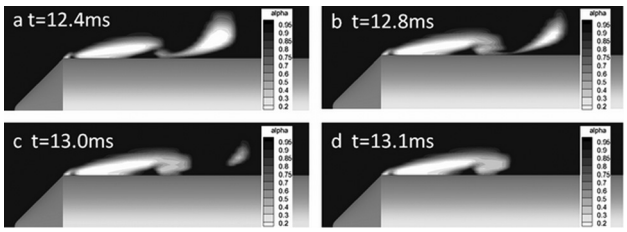

Fig. 16 Collapse of shedding bubble in simulation

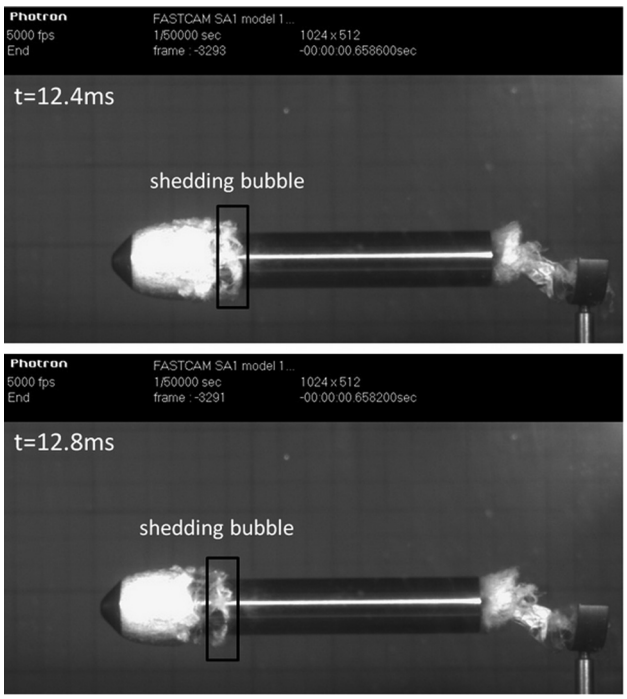

Fig. 17 Collapse of shedding bubble in experiment

the cavity that is not separated totally in Fig. 6(*f*) ends at B. In Figs. 6(*g*) and 6(*h*), the cavity is departed totally and the shedding part becomes small, so the cavity closes at C/D. In Fig. 6, the arrows stand for the length of the cavity. As shown in Fig. 7, L/d_1 obtained from the experiment and numerical simulation agrees well with each other.

In the results and analysis above, unsteady evolution of cavitation is related closely to the re-entry jet. Therefore, the formation and development of the re-entry jet are described in the following analysis.

4.2 Formation and Development of Re-entry Jet. Unsteady cavitation and re-entrant jet have been widely studied. De Lange and De Bruin [16] and Sayyaadi [17] performed experiments on cavitation by means of high-speed video too. De Lange and De Bruin [16] observed two-dimensional as well as three-dimensional cavities. From the observation, it is concluded that the formation of a re-entrant jet is of major importance to explain the unsteadiness. Sayyaadi [17] analyzed images using the light intensity comparison technique, and the cavitation length for each image was evaluated. He also observed that, at lower cavitation numbers, periodic separation, shedding, and collapsing of the cloudlike cavities are observed together with the re-entrant jet motion. The structure of the two-phase flow inside the cavity was investigated by Stutz and Reboud [18] using a double optical probe. They succeeded in measuring the local void fraction and the velocity inside their cavities. The measurements show an extended reversed flow occurring along the solid surface, which plays a significant function in the vapor cloud shedding process. An ultrasonic technique was developed by Callenaere et al. [19] to measure the thickness of the liquid layer that lies just below the cavity. They also used laser Doppler velocimeter (LDV) to measure the horizontal flow velocity at different stations along the channel and to compute the pressure gradient from the following relation. Their investigations give insight into the instabilities that a partial cavity may undergo and particularly the re-entrant jet instability. Other experimental techniques were used to investigate the instability of cloud cavities, such as X-ray imaging technique (Dular et al. [20] and Stutz and Legoupil [21]).

In cavitation, re-entry jet and cavity influence each other. In the present paper, cavity forms at the shoulder firstly. Figure 8 shows the flow field at the cavity closure at the beginning. The velocity of whole field is in the same direction with the incoming flow. The re-entry hasn't formed yet. However, the pressure outside the closure is high, corresponding to the low-pressure field in the cavity. There is obvious adverse pressure gradient. At the continuous impact of adverse pressure gradient, the mixture's velocity will decrease. Because of viscosity, the velocity of the fluid in the boundary layer will reduce to zero first. Then, it will flow in the opposite direction. That is the re-entry jet, as shown in Fig. 9. However, in field away from the wall, the flow moves forward still. That is the boundary-layer separation phenomenon, as shown in Fig. 10. The separation point is located near point (*c*). The flow direction of the fluid near the wall is the same with the incoming flow before (*c*) and opposite in the separation field after (*c*).

The re-entry jet moves into the cavity after its generation. Before that, the cavity is uniformly transparent, as shown in Fig. 11. Figures 12 and 13 show re-entrant jet in experiment and simulation, respectively. When re-entrant jet gets into the cavity, the transparent cavity is disturbed and generates tiny foam, as shown in Fig. 12. Re-entrant jet under the cavity corresponds to the brightest pixels in the image. In Fig. 13, the mixture in which the water volume fraction α is more than 70% and velocity is less than 0 is thought to be re-entrant jet. The length of re-entrant jet and cavity are l and L, respectively. The dimensionless quantity l/L in simulation and experiment are consistent, as shown in Fig. 14. As shown in the figures, the re-entry jet moves in the cavity until it reaches the forepart of the projectile. Then, the re-entry jet rolls back in an uptrend with the incoming flow. This rolled back re-entrant jet cuts off the cavity, inducing the shedding of bubble.

4.3 Evolution of Shedding Bubble. Shedding bubble induced by re-entry jet is important behavior of cloud cavitation's instability. At the beginning of this process, the bubble is near the re-entry jet and attached to the wall, as shown in Fig. 15(*a*).

As the shedding bubble moves backwards, the re-entry jet between it and the wall weakens and meets the incoming flow at the left end of the bubble. Then, the re-entry jet flows back, which induces the backrush of the shedding bubble too. The bubble whose cross section changes from ellipse into circular gradually gets apart with the wall, as shown in Figs. 15(*b*)–15(*d*).

Then, the bubble flows into the high-pressure area. It will reattached to the wall again, as shown in Fig. 15(*e*). The bottom of the bubble, which is near to the re-entry jet, is at a lower speed than the top part. So the cross section of the bubbles changes into oblateness with wrapping angle.

Finally, as shown in Fig. 16, when the bubble is far away from the shoulder, it behaves as a single bubble without any influence of re-entry jet and cavitation ahead. It lasts 1.2 ms until the bubble collapses. That is acceptable compared to 0.8 ms in experiment, as shown in Fig. 17.

In general, affected by the re-entry jet and incoming flow, the shedding bubble attaches, detaches, and reattaches with the wall until it collapses in the flow field. The cross section of it changes in this process too.

5 Concluding Remarks

We have studied the natural cavitation around axisymmetric projectile using the LES method above. LES has the ability to describe medium-scale to small-scale flow structures, which is essential to reveal mechanisms in cavitation.

Periodic bubble shedding, which is thought to be closely related to re-entry jet, is observed in both numerical and experimental results. Re-entry jet induced by adverse pressure gradient flows into cavity and rolls back in an uptrend at the forepart of the projectile. Then, cavity is cut off by the re-entrant jet, leading to bubble shedding. Affected by the re-entry jet and main flow, the shedding bubble attaches, detaches, and then reattaches with the wall until it collapses.

To conclude, LES is a powerful and reliable tool for understanding the phenomenon of cavitation. The above has discussed some mechanism in it. However, there is still much further work needed to be done on cavitation, such as the pressure and drag the projectile is faced with.

Acknowledgment

This research was sponsored by National Natural Science Foundation of China under Contract 11332011 (Chenguang Huang, Program Manager) and 11202215 (Yiwei Wang, Program Manager).

References

[1] Franc, J. P., and Michel, J. M., 2004, *Fundamentals of Cavitation*, Kluwer Academic, Dordrecht, The Netherlands.

[2] Seo, J. H., Moon, Y. J., and Shin, B. R., 2008, "Prediction of Cavitating Flow Noise by Direct Numerical Simulations," J. Comput. Phys., **227**, pp. 6511–6531.

[3] Plesset, M. S., and Prosperetti A., 1977, "Bubble Dynamics and Cavitation," Annu. Rev. Fluid Mech., **9**, pp. 145–185.

[4] Singhal, A. K., Athavale, M. M., Li, H., and Jiang, Y., 2002, "Mathematical Basis and Validation of the Full Cavitation Model," ASME J. Fluids Eng., **124**, pp. 617–624.

[5] Dular, M., Bachert, R., Stoffel, B., and Širok, B., 2005, "Experimental Evaluation of Numerical Simulation of Cavitating Flow Around Hydrofoil," Eur. J. Mech.- B/Fluids, **24**, pp. 522–538.

[6] Huang, B., Wang, G. Y., Zhang, B., and Yu, Z., 2009, "Evaluation of the Cavitation Models on the Numerical Simulation of Cloud Cavitating Flows Around a Hydrofoil," Trans. Beijing Inst. Technol., **29**, pp. 785–789.

[7] Ji, B., Luo, X. W., Peng, X. X., Wu, Y. L., and Xu, H. Y., 2010, "Numerical Analysis for Three Dimensional Unsteady Cavitation Shedding Structure Over a Twisted Hydrofoil," Chin. J. Hydrodyn., **25**, pp. 217–223.

[8] Bensow, R. E., and Bark, G. R., 2010, "Implicit LES Predictions of the Cavitating Flow on a Propeller," ASME J. Fluids Eng., **132**, p. 041302.

[9] Bensow, R. E., and Bark, G., 2010, "Simulating Cavitating Flows With LES in OpenFOAM," V European Conference on Computational Fluid Dynamics.

[10] Wang, G., and Ostoja-Starzewski, M., 2007, "Large Eddy Simulation of a Sheet/Cloud Cavitation on a NACA0015 Hydrofoil," Appl. Math. Model., **31**, pp. 417–447.

[11] Passandideh Fard, M., and Roohi, E., 2008, "Transient Simulations of Cavitating Flows Using a Modified Volume-of-Fluid (VOF) Technique," Int. J. Comput. Fluid Dyn., **22**(1-2), pp. 97–114.

[12] Fox, R. O., 2012, "Large-Eddy-Simulation Tools for Multiphase Flows," Annu. Rev. Fluid Mech., **44**(1), pp. 47–76.

[13] Kunz, R. F., Boger, D. A., Stinebring, D. R., Chyczewski, T. S., Lindau, J. W., Gibeling, H. J., Venkateswaran, S., and Govindan, T. R., 2000, "A Preconditioned Navier–Stokes Method for Two-Phase Flows With Application to Cavitation Prediction," Comp. Fluids, **29**, pp. 849–875.

[14] Liu, D. M., Liu, S. H., Wu, Y. L., and Xu, H. Y., 2009, "LES Numerical Simulation of Cavitation Bubble Shedding on ALE 25 and ALE 15 Hydrofoils," J. Hydrodyn., **21**, pp. 807–813.

[15] Wei, Y. P., Wang, Y. W., Fang, X., Huang, C. G., and Duan, Z. P., 2011, "A Scaled Underwater Launch System Accomplished by Stress Wave Propagation Technique," Chin. Phys. Lett., **28**, p. 024601.

[16] De Lange, D. F., and De Bruin, G. J., 1997, "Sheet Cavitation and Cloud Cavitation, Re-entrant Jet and Three-dimensionality," *Fascination of Fluid Dynamics*, Springer, Dordrecht, The Netherlands, pp. 91–114.

[17] Sayyaadi, H., 2010, "Instability of the Cavitating Flow in a Venturi Reactor," Fluid Dyn. Res., **42**, p. 055503.

[18] Stutz, B., and Reboud, J., 1997, "Experiments on Unsteady Cavitation," Exp. Fluids, **22**, pp. 191–198.

[19] Callenaere, M., Franc, J. P., Michel, J. M., and Riondet, M., 2001, "The Cavitation Instability Induced by the Development of a Re-entrant Jet," J. Fluid Mech., **444**, pp. 223–256.

[20] Dular, M., Khlifa, I., Fuzier, S., Maiga, M. A., and Coutier-Delgosha, O., 2012, "Scale Effect on Unsteady Cloud Cavitation," Exp. Fluids, **53**, pp. 1233–1250.

[21] Stutz, B., and Legoupil, S., 2003, "X-ray Measurements Within Unsteady Cavitation," Exp. Fluids, **35**, pp. 130–138.